ChemComm

COMMUNICATION

View Article Online
View Journal | View Issue

Cite this: *Chem. Commun.*, 2023, 59, 5407

Received 17th February 2023,
Accepted 4th April 2023

DOI: 10.1039/d3cc00763d

rsc.li/chemcomm

Simultaneously controlling conformational and operational stability of single-chain polymeric nanoparticles in complex media†

Stefan Wijker, Rico Monnink, Luc Rijnders, Linlin Deng and Anja R.A. Palmans *

Single-chain polymeric nanoparticles (SCPNs) comprising a solvatochromic pyrazoline adduct show conformational and operational stability in complex media and in cellular compartments; the connectivity of the adduct is crucial in modulating interactions with the surrounding media.

Folding single chains of amphiphilic heterograft copolymers into single-chain polymeric nanoparticles (SCPNs) of defined size and shape is a promising approach towards utilizing these synthetic polymers in bio-applications such as (cell) imaging,[1–6] bio-orthogonal catalysis,[7–12] and preservation of protein function.[13] Two important factors regulate the successful application of SCPNs in complex media. First, there is a need for high conformational stability, wherein the SCPNs have the ability to retain size and compartmentalized shape. Second, SCPNs need good functional stability, whereby good performance over time is retained. Achieving this is not trivial, as interactions with hydrophobic proteins and peptides present in complex media affect stability and reduce performance.[1] This has been highlighted by significant reductions in the activity of bio-orthogonal catalysts embedded in SCPNs when used in complex media.[12,14]

Recently, we showed that SCPNs with high conformational stability in complex media can be prepared by the introduction of covalent cross-links *via* coumarin dimerization after folding of the polymer chains *via* hydrophobic and hydrogen-bonding interactions.[15] Since the fluorescence of the coumarin was lost after dimerization, the solvatochromic dye Nile Red was separately introduced to track the SCPNs in living cells and report on the presence of dye–cell interactions through solvatochromic shifts.[1] We concluded that a covalent connectivity of the Nile Red to the polymer was crucial to reduce interactions with hydrophobic proteins in the cell culturing media. However, the need to covalently attach a fluorescent dye makes the synthesis of SCPNs more demanding.

Here, we set out to develop SCPNs that have the crosslinking and reporter function unified in one motif. We selected the nitrile imine-mediated tetrazole-ene cycloaddition, NITEC, which is a light-triggered, irreversible "click" reaction that proceeds at high reaction rates and without the need of a catalyst.[16] The NITEC reaction was elegantly used by Barner-Kowollik and co-workers to intramolecularly crosslink polymers to SCPNs both in organic as well as in aqueous media.[17–19] Interestingly, the NITEC reaction affords a fluorescent pyrazoline adduct.[20,21] This adduct has been studied as a promising fluorophore in protic solutions,[22] and for its solvatochromic properties.[23] We show in this work that the solvatochromic properties of pyrazoline adduct can be transferred to provide a reporter function for SCPNs in complex media and living cells. Measuring the changes in the emission spectra resulting from interactions between the adduct and the surrounding media will permit to understand both the conformational as well as functional stability of SCPNs in complex media and living cells.

Three different polymers **P1–P3** were prepared *via* RAFT copolymerization of hydrophobic and hydrophilic methacrylate derivatives (Scheme 1): oligo(ethylene glycol) (oEG) modified methacrylate to ensure water solubility, *n*-dodecyl (Dod) methacrylate to drive the hydrophobic collapse of the polymer in water, and methacrylates functionalized with either a furan-protected maleimide (pMal) or a tetrazole (Tet) moiety that act as the two precursors for the pyrazoline formation *via* the NITEC reaction. As the adduct connectivity is an important factor when considering SCPN interactions with surrounding media, we designed polymer **P1–P3** to possess different microstructures. Apart from oEG and Dod grafts, **P1** comprised both pMal and Tet grafts, each about 4%. **P2** had no additional grafts, and **P3** comprised only pMal grafts (4%). The RAFT synthesis resulted in polymers with incorporation ratios in good agreement with the feed ratios, a degree of polymerization (DP) between 150 and 200, and a relatively narrow molar mass dispersity (*Đ* around 1.3). The synthesis and characterization are described in detail in the ESI†

Institute for Complex Molecular Systems, Laboratory of Macromolecular and Organic Chemistry, Eindhoven University of Technology, P.O. Box 513, 5600 MB, Eindhoven, The Netherlands. E-mail: a.palmans@tue.nl

† Electronic supplementary information (ESI) available: Materials and methods, experimental section, and additional characterization. See DOI: https://doi.org/10.1039/d3cc00763d

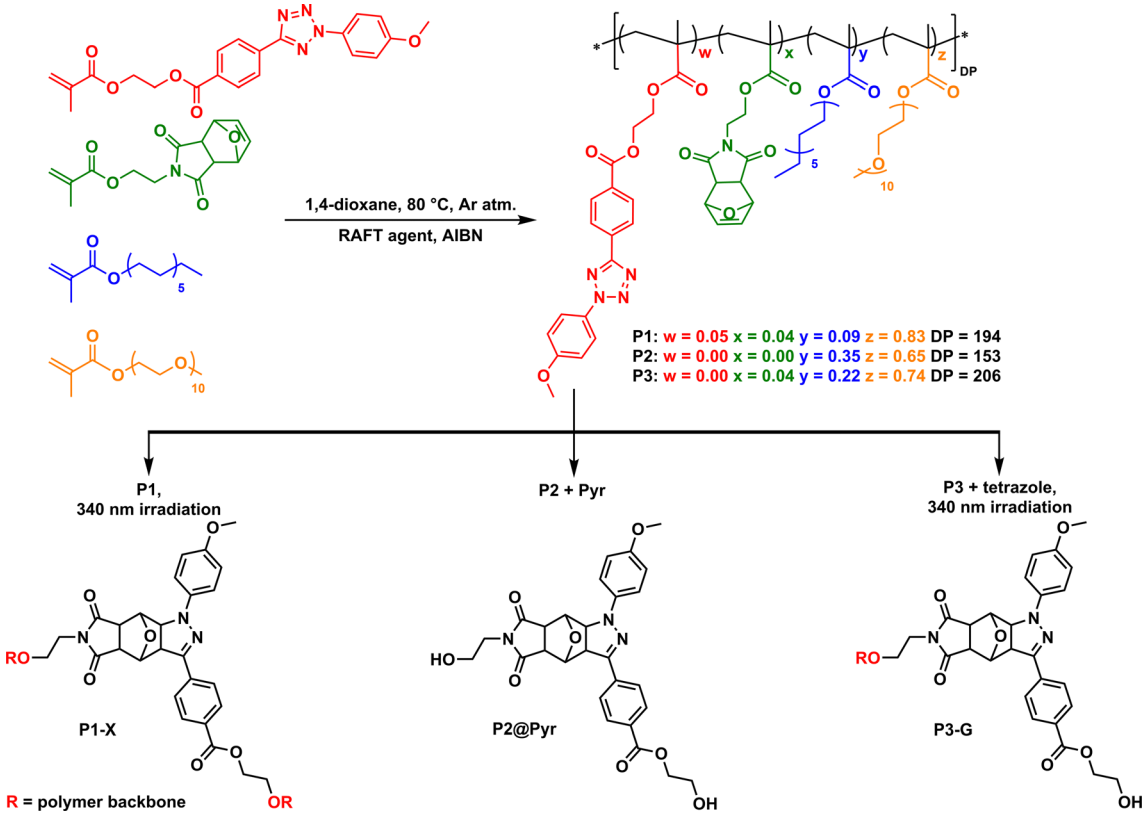

Scheme 1 Structures of **P1–P3** prepared *via* RAFT copolymerization of different monomers (top). Irradiation of **P1** gives pyrazoline crosslinks resulting in **P1-X** (bottom left). Encapsulation of free pyrazoline adduct **Pyr** in **P2** forms **P2@Pyr** (bottom middle). Irradiation of **P3** with free tetrazole leads to **P3-G** with pyrazoline dangling grafts (bottom right).

(Section 2.2). All polymers readily dissolve in water and form nanoparticles with a small, defined size, with hydrodynamic radii R_H between 6 and 8 nm as determined by dynamic light scattering (DLS) (see ESI,† Section 2.3).

P1, including both pMal and Tet, was crosslinked in water at dilute conditions (c_{pol} = 1 mg mL^{-1}) using irradiation with UV-light (λ = 340 nm, irradiance = 4 mW cm^{-2}). This affords predominantly intramolecularly formed pyrazoline adducts (**P1-X**) as verified by DLS measurements (Scheme 1, bottom left, see ESI,† Section 2.3). The polymer concentration was kept low to suppress intermolecular cross-linking. **P2** is used for the physical encapsulation of free pyrazoline adduct (**Pyr**) resulting in **P2@Pyr**. **Pyr** was synthesized separately, see Scheme 1 bottom middle, and we determined a fluorescence quantum yield Φ_{pyr} of 0.128 (see ESI† Section 2.4–2.6 for details). **P3** contains pMal but no Tet grafts. Addition of free tetrazole and subsequent UV-light irradiation in water resulted in the formation of pyrazoline grafts connected to the polymer backbone *via* the maleimide moiety as dangling chains (**P3-G**) (Scheme 1, bottom right).

We first evaluated the solvatochromic behaviour of free **Pyr** (Scheme 1 and Fig. S26, ESI†) in solvents that differ in polarity. A bathochromic shift in the emission maxima from 500 nm in apolar *p*-xylene to 550 nm in polar acetic acid is observed (see ESI,† Section 2.5). This large shift indicates that **Pyr** can be used as a reporter to probe the polarity of its microenvironment when incorporated in SCPNs. Next, we probed the formation of the pyrazoline adduct in water for **P1** and **P3** using absorbance and fluorescence spectroscopy. Fig. 1A shows the absorbance spectrum over time during the NITEC reaction on **P1**. The decrease in absorbance around 300 nm corresponds to the disappearance of the tetrazole and the new bands appearing around 250 and 410 nm correspond to successful pyrazoline formation (see ESI,† Section 2.6). The conversion of the precursors into pyrazoline as a function of time was calculated *via* the feed ratios and the pyrazoline extinction coefficient (see ESI,† section 2.7) and is quantified in Fig. 1B, reaching 56% conversion after 105 minutes. For **P1**, 105 minutes was the optimum irradiation time, resulting in **P1-X** with, on average, 4.3 crosslinks per chain. Longer irradiation times lead to a net decrease in the amount of pyrazoline as the pyrazoline absorbance peak starts to decrease again, possibly due to photooxidation of the adduct.[24] Formation of pyrazoline adducts in **P3** proceeded similarly to **P1**, reaching a maximum pyrazoline concentration for **P3-G** after five hours irradiation at 66% conversion before a decrease of the pyrazoline absorption sets in. This corresponds to 5.4 grafts per chain. The absorbance and fluorescence spectra showed no significant changes after storing the polymer solutions for three months at ambient conditions, indicating that there is no dye degradation over time (see ESI,† Section 2.8). This highlights the excellent long-term stability of the pyrazoline adducts embedded in the amphiphilic polymers in water.

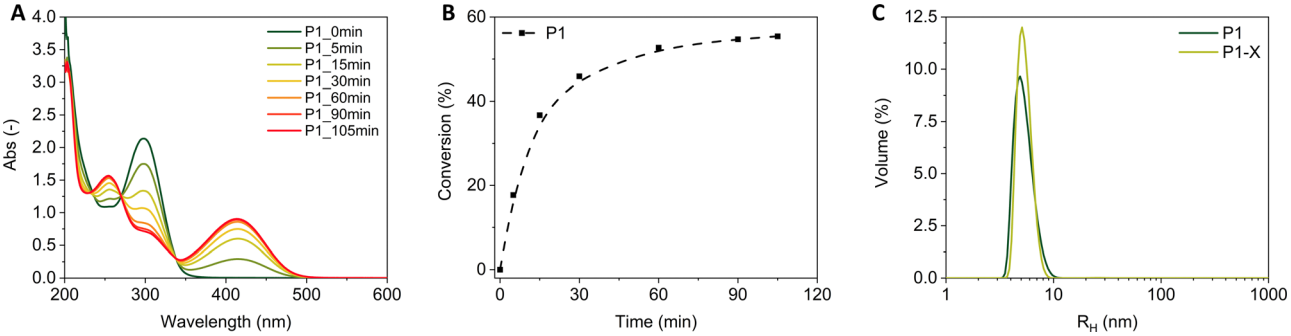

Fig. 1 (A) Evolution of absorbance spectra during photoirradiation of **P1** in water. c_{pol} = 1 mg mL^{-1}. (B) Conversion of pMal into pyrazoline adduct over time. The dashed line is added to guide the eye. (C) Volume distribution of hydrodynamic radii (R_H) of **P1** before (**P1**) and after photoirradiation (**P1-X**) as measured by DLS. c_{pol} = 1 mg mL^{-1}.

With **P1-X** and **P3-G** successfully prepared, we set out to investigate the interactions of the different polymer systems at high concentrations (c_{pol} = 3 mg mL^{-1}) with complex media. To this end, the fluorescence spectra in water—without competing interactions—were compared to those in a 10 : 90 vol% mixture of fetal bovine serum (FBS) and Dulbecco's modified eagle medium (DMEM). Fig. 2 shows an identical shape of the fluorescence spectra and no shift in the fluorescence maxima (543 nm for **P1-X**, and 537 nm for **P2@Pyr** and **P3-G**) when going from water to cell culture medium. It follows from these observations that the pyrazoline remains trapped inside the SCPNs and does not interact with the FBS proteins. This is likely caused by the insolubility of the pyrazoline adduct in water, see ESI,† Section 2.5 for details. As the systems are stable in cell culture medium, **P1-G**, **P2@Pyr** and **P3-G** were incubated with HeLa cells for 24 h with 10 : 90 vol% FBS:DMEM solutions (c_{pol} = 3 mg mL^{-1}) in order to probe polymer–cell interactions. After successful internalization of the 3 polymers in the HeLa cells, confocal microscopy was used to visualize the cells and determine the fluorescence spectrum of the pyrazoline adducts (Fig. 3). Polymers **P1-X** and **P3-G** are internalized by cells, giving a dots-like cluster, whereas the free pyrazoline adduct of **P2@Pyr** seems to have been distributed homogeneously throughout the cytoplasm. The fluorescence spectra reveal that **P1-X**, in which the pyrazoline adduct acts as a cross-link, shows near identical fluorescence spectra in FBS and HeLa cells, indicating the absence of interactions. For **P3-G**, a blue-shift is observed in HeLa cells, which means that pyrazoline as dangling unit instead of as cross-link interacts with the cellular constituents. Finally, the largest blue-shift in HeLa cells is observed for **P2@Pyr**, indicating that the free pyrazoline adduct likely escapes from the SCPN and interacts with hydrophobic constituents, hereby showing the highest amount of interaction with the environment. The results for **P1-X** highlight that solvatochromic pyrazoline adducts act as stabilizing crosslinks for SCPN formation, and replaces the need for attaching fluorescent tracking moieties such as Nile Red. Analogous to what was observed for Nile Red,[1] covalently linking the pyrazoline to the polymer backbone reduces interactions between the probe and its surroundings. But, the type of connectivity between the polymer and the pyrazoline matters, since the cross-linked adduct shows less interaction.

In summary, the NITEC reaction is a promising approach to include conformationally and functionally stabilizing fluorescent covalent cross-links in SCPNs. This method allows particle tracking *via* fluorescence without the need to incorporate additional fluorescent probes. Additionally, the fluorescence of the pyrazoline adduct is stable for a long time and no shift in the fluorescence maxima was observed in FBS:DMEM, corroborating both operational and conformational stability. In the presence of HeLa cells, the connectivity of the pyrazoline probe and the polymer is important as pyrazoline cross-links introduce additional stability to the polymer particles compared to dangling chains. Both approaches outperform free pyrazoline incorporated into cells *via* hydrophobic interactions. As such,

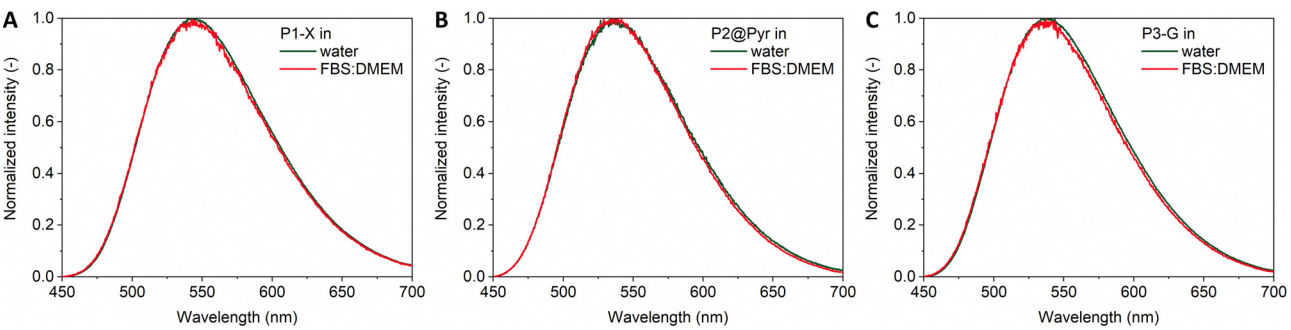

Fig. 2 Normalized fluorescence spectra of (A) **P1-X**, (B) **P2@Pyr**, and (C) **P3-G** in water and 10 : 90 vol% FBS:DMEM (c_{pol} = 3 mg mL^{-1}, c_{pyr},**P1-X** = 140 μM, c_{pyr},**P2@Pyr** = 20 μM, c_{pyr},**P3-G** = 150 μM, λ_{ex} = 405 nm).

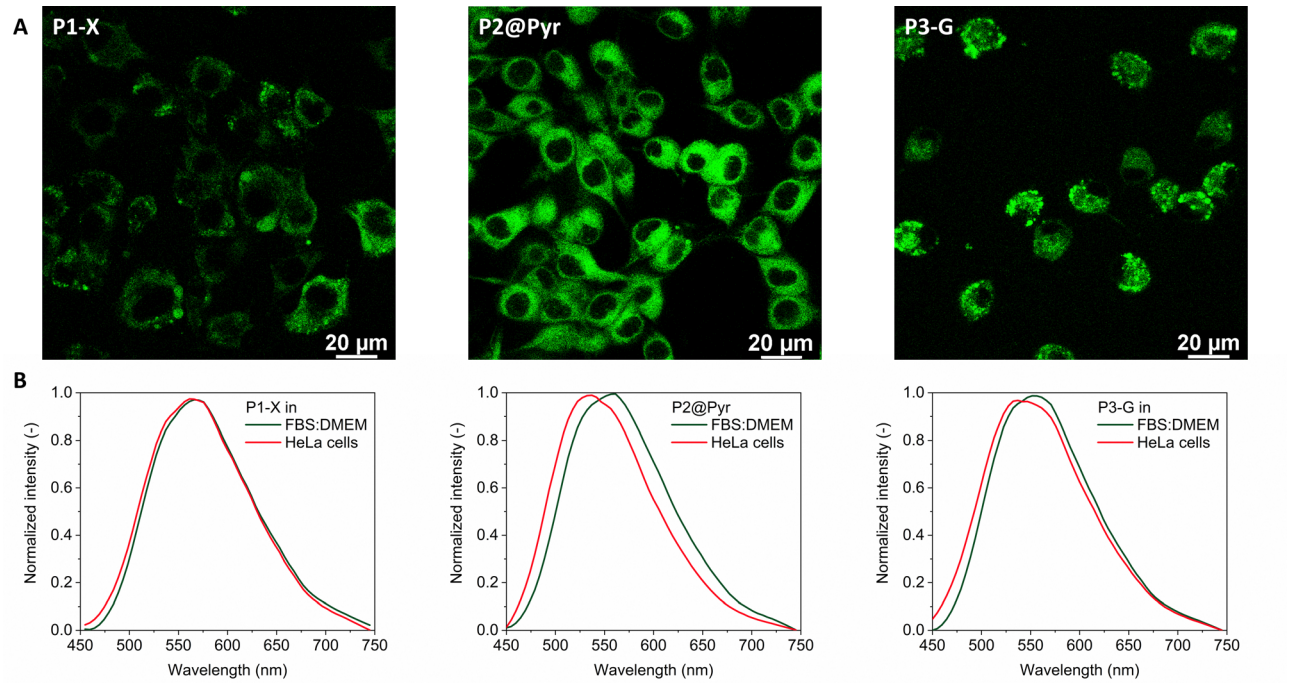

Fig. 3 (A) Confocal microscopy images of **P1-X**, **P2@Pyr**, and **P3-G** in HeLa cells after 24 h incubation and (B) the corresponding fluorescence spectra in 10 : 90 vol% FBS:DMEM and in HeLa cells (c_{pol} = 3 mg mL^{-1}, c_{pyr},**P1-X** = 140 μM, c_{pyr},**P2@Pyr** = 20 μM for **P1**, c_{pyr},**P3-G** = 150 μM, λ_{ex} = 405 nm).

the pyrazoline adduct reveals the influence of polymer architecture on cell interactions and gives guidelines for the future design of conformationally and functionally stable SCPNs for biological applications with excellent long-term stability. This novel approach to SCPN formation permits to design stable and traceable SCPNs that act as carriers for bioorthogonal catalysts in complex media, which is the topic of future investigations.

This research was financed by the Dutch Ministry of Education, Culture and Science (Gravity program 024.001.035), and the European Union's Horizon 2020 research and innovation program under the Marie Sklodowska-Curie Grant Agreement no. 765497 (THERACAT).

Conflicts of interest

There are no conflicts to declare.

Notes and references

1 L. Deng, L. Albertazzi and A. R. A. Palmans, *Biomacromolecules*, 2022, **23**, 326–338.
2 A. P. P. Kröger and J. M. J. Paulusse, *J. Controlled Release*, 2018, **286**, 326–347.
3 I. Perez-Baena, I. Loinaz, D. Padro, I. García, H. J. Grande and I. Odriozola, *J. Mater. Chem.*, 2010, **20**, 6916–6922.
4 R. Gracia, M. Marradi, U. Cossío, A. Benito, A. Pérez-San Vicente, V. Gómez-Vallejo, H. J. Grande, J. Llop and I. Loinaz, *J. Mater. Chem. B*, 2017, **5**, 1143–1147.
5 A. B. Benito, M. K. Aiertza, M. Marradi, L. Gil-Iceta, T. Shekhter Zahavi, B. Szczupak, M. Jiménez-González, T. Reese, E. Scanziani, L. Passoni, M. Matteoli, M. De Maglie, A. Orenstein, M. Oron-Herman, G. Kostenich, L. Buzhansky, E. Gazit, H.-J. J. Grande, V. Gómez-Vallejo, J. Llop and I. Loinaz, *Biomacromolecules*, 2016, **17**, 3213–3221.
6 M. Collot, J. Schild, K. T. Fam, R. Bouchaala and A. S. Klymchenko, *ACS Nano*, 2020, **14**, 13924–13937.
7 K. Liu, Y. Tian, R. Pitchimani, M. Huang, H. Lincoln and D. Pappas, *Talanta*, 2009, **79**, 333–338.
8 J. Chen, K. Li, S. E. Bonson and S. C. Zimmerman, *J. Am. Chem. Soc.*, 2020, **142**, 13966–13973.
9 E. S. Garcia, T. M. Xiong, A. Lifschitz and S. C. Zimmerman, *Polym. Chem.*, 2021, **12**, 6755–6760.
10 J. Chen, J. Wang, K. Li, Y. Wang, M. Gruebele, A. L. Ferguson and S. C. Zimmerman, *J. Am. Chem. Soc.*, 2019, **141**, 9693–9700.
11 Y. Deng, T. Wu, X. Chen, Y. Chen, Y. Fei, Y. Liu, Z. Chen, H. Xing and Y. Bai, *J. Am. Chem. Soc.*, 2023, **145**, 1262–1272.
12 A. Sathyan, S. Croke, A. M. Pérez-López, B. F. M. de Waal, A. Unciti-Broceta and A. R. A. Palmans, *Mol. Syst. Des. Eng.*, 2022, **7**, 1736–1748.
13 B. Panganiban, B. Qiao, T. Jiang, C. DelRe, M. M. Obadia, T. D. Nguyen, A. A. A. Smith, A. Hall, I. Sit, M. G. Crosby, P. B. Dennis, E. Drockenmuller, M. Olvera de la Cruz and T. Xu, *Science*, 2018, **359**, 1239–1243.
14 Y. Liu, S. Pujals, P. J. M. Stals, T. Paulöhrl, S. I. Presolski, E. W. Meijer, L. Albertazzi and A. R. A. Palmans, *J. Am. Chem. Soc.*, 2018, **140**, 3423–3433.
15 S. Wijker, L. Deng, F. Eisenreich, I. K. Voets and A. R. A. Palmans, *Macromolecules*, 2022, **55**, 6220–6230.
16 J. S. Clovis, A. Eckell, R. Huisgen and R. Sustmann, *Chem. Ber.*, 1967, **100**, 60–70.
17 C. Heiler, J. T. Offenloch, E. Blasco and C. Barner-Kowollik, *ACS Macro Lett.*, 2017, **6**, 56–61.
18 C. Heiler, S. Bastian, P. Lederhose, J. P. Blinco, E. Blasco and C. Barner-Kowollik, *Chem. Commun.*, 2018, **54**, 3476–3479.
19 J. T. Offenloch, J. Willenbacher, P. Tzvetkova, C. Heiler, H. Mutlu and C. Barner-Kowollik, *Chem. Commun.*, 2017, **53**, 775–778.
20 R. Huisgen, M. Seidel, G. Wallbillich and H. Knupfer, *Tetrahedron*, 1962, **17**, 3–29.
21 R. Huisgen, *Angew. Chem., Int. Ed.*, 1963, **2**, 565–598.
22 Y.-K. Zhang, M. Li, L. Ruan and P. An, *Chem. Commun.*, 2022, **58**, 10404–10407.
23 K. A. Haupa, A. Szukalski and J. Myśliwiec, *J. Phys. Chem. A*, 2018, **122**, 7808–7818.
24 M. Soltani, H. R. Memarian and H. Sabzyan, *J. Photochem. Photobiol., A*, 2020, **389**, 112285.

